# Solvothermal-assisted evaporation-induced self-assembly process for significant improvement in the textural properties of γ-Al$_2$O$_3$, and study dye adsorption efficiency

CrossMark

Sourav Ghosh, Pallab Bose, Somjyoti Basak, Milan Kanti Naskar*

*Sol-Gel Division, CSIR-Central Glass and Ceramic Research Institute, Kolkata 700 032, India*

ABSTRACT

A comparative study of the textural properties of γ-Al$_2$O$_3$ prepared by solvothermal-assisted evaporation-induced self-assembly (SA-EISA) and conventional evaporation-induced self-assembly (EISA) processes has been carried out using aluminum isopropoxide, triblock copolymer-type nonionic surfactant (Pluronic P123) and ethanol. The solvothermal reaction was carried out at 100 °C for 24 h followed by slow drying at 60 °C for 48 h. The synthesized products were characterized by thermogravimetry analysis (TGA), differential thermal analysis (DTA), X-ray diffraction (XRD) analysis, N$_2$ adsorption–desorption study and transmission electron microscopy (TEM). The γ-Al$_2$O$_3$ prepared by SA-EISA process became stable up to 1000 °C. The powder prepared by SA-EISA process resulted in a significant increase in textural properties (BET surface area, pore volume and pore diameter) compared to that prepared by conventional EISA process. A better adsorption capacity for Congo red, a carcinogenic dye used in textile industry, was exhibited by the powders prepared by SA-EISA process. A proposed mechanism was illustrated for the formation of mesoporous γ-Al$_2$O$_3$ obtained by EISA and SA-EISA processes.

© 2015 The Ceramic Society of Japan and the Korean Ceramic Society. Production and hosting by Elsevier B.V. All rights reserved.

## 1. Introduction

The discovery of ordered mesoporous silica (the M41S family) [1] using templates with surfactant assemblies has been a breakthrough in the research field for its potential applications in catalysis and in other realms of chemistry. In extension, the efforts have been made for the synthesis of other groups of mesoporous oxides in nonsilica systems. In comparison to mesoporous silica, mesoporous alumina (MA) is important for its wide applications as adsorbents, catalysts, catalyst supports, membranes, ceramics, etc. The first successful synthesis of ordered mesoporous alumina was reported by Vaudry et al. [2] using long-chain carboxylic acids as the structure directing agents. For preparing MA, many other synthesis routes like sol–gel [3], aerosol generation of particles using block copolymers [4], cationic [5] and anionic surfactants [2], block copolymers [6,7], mesoporous carbon templates [8], colloidal precursors with amine-based structural agents [9], *Stevia rebaudiana*

leaves extract as templating agent [10], spray pyrolysis method [11], etc. have been developed. Glucose has been used for enhancement of porosity and surface area of alumina [12]. Recently, we have reported the role of tetramethyl urea for the synthesis of mesoporous alumina [13]. The MA was also obtained by normal evaporation-induced self-assembly (EISA) method using aluminum alkoxides and triblock copolymers as surfactants [14]. However, the influence of solvothermal reaction in the conventional EISA process has not yet been reported earlier.

The potential applications of alumina depend upon its structural, textural and morphological characteristics. There has been a great interest in obtaining mesoporous alumina (MA) with high surface area, large pore volumes, crystalline pore walls, and good thermal stability for favorable enhancement of catalytic and adsorptive performances. The porosity of the materials depends on the way the hydrolysis-polycondensation reaction of aluminum alkoxides with the aid of co-assembly of surfactant [15] occurs. The nature of interactions between polymerizing inorganic species and surfactant molecules is important in tailoring the porosity and pore structures of mesoporous alumina. Hydrothermal reaction significantly improved the textural properties of SBA-15 [16].

Environmental problem relating to the water pollution is a challenging issue in recent time. The pollution of water resources by

* Corresponding author. Tel.: +91 33 2473 3496x3516; fax: +91 33 2473 0957.
*E-mail address:* milan@cgcri.res.in (M.K. Naskar).
Peer review under responsibility of The Ceramic Society of Japan and the Korean Ceramic Society.

dyes from textiles and mining industries has become a serious concern. It is worth mentioning that the textural and framework properties related to surface area, pore volume, porosity, pore size distribution (PSD), and ordering of the pores of alumina could affect on its adsorption behaviors toward the removal of toxic and carcinogenic dyes, Congo red (CR). Recently we have studied the adsorption efficiency for Congo red with the nanostructured mesoporous alumina synthesized from boehmite sol [17,18].

Keeping this view in mind, in the present investigation we have studied the solvothermal effect on the synthesis of mesoporous $\gamma$-$Al_2O_3$ by EISA process, in terms of crystallization, textural properties, and adsorption efficiency for CR removal. A comparative study was performed in the absence of solvothermal reaction (conventional EISA process). To the best of our knowledge, it is the first time we report the significant improvements of textural properties as well as CR adsorption efficiency of mesoporous alumina synthesized by solvothermal-assisted EISA process.

## 2. Experimental

### 2.1. Material preparation

Aluminum isopropoxide, Congo red (CR) and triblock copolymer (Pluronic P123) were purchased from Sigma–Aldrich Co. (USA). Absolute ethyl alcohol and nitric acid were from Merck (India). All reagents were used as received.

In a typical experiment, 1.6 g of P123 was dissolved in 40 mL of ethyl alcohol under stirring at 35 °C for 60 min. Then 4.16 g of aluminum isopropoxide dissolved in 40 mL of ethyl alcohol and 2.8 mL of 67 wt% nitric acid was added into the former solution. The mix solution was allowed to stir for 5 h to obtain a homogeneous sol. The above sol was divided into two parts. One part of the sol was poured into a petri dish and kept in an oven at 60 °C for 48 h for solvent evaporation (EISA process). Another part of the sol was poured into a Teflon-lined autoclave and kept at 100 °C for 24 h followed by natural cooling. A gelly-like mass (wet gel) was obtained after solvothermal treatment. It was then put in an oven at 60 °C for 48 h to evaporate the solvent as done in normal EISA process. The second process was termed as solvothermal-assisted EISA (SA-EISA) process. To optimize the effect of solvothermal reaction temperature on the textural properties of powders, the SA-EISA process was repeated at 80 °C and 130 °C. The dried powders obtained from both the EISA and SA-EISA processes were calcined at 400 °C for 4 h with a heating rate of 1 °C min$^{-1}$, and at 700 °C, 900 °C, 1000 °C, 1100 °C with a heating rate of 1 °C min$^{-1}$ up to 400 °C/4 h followed by heating rate of 5 °C min$^{-1}$ up to those temperatures with 1 h dwell time each.

### 2.2. Characterization

The thermal behaviors of the prepared powders were studied by differential thermal analysis (DTA) and thermogravimetry analysis (TGA) (NETZSCH, STA 449C) up to 1000 °C in air atmosphere at the heating rate of 10 °C min$^{-1}$. The wide-angle XRD measurements were performed for calcined samples using powder diffraction technique by a Philips X'Pert Pro XRD (Model: PW 3050/60) with Ni-filtered Cu-K$_\alpha$ radiation ($\lambda$ = 0.15418 nm), operating at 40 kV and 30 mA. The low-angle XRD measurements of the calcined samples (400 °C) were recorded by Rigaku Smartlab (9 kW) using Cu-K$_\alpha$ radiation, operating at 45 kV and 200 mA. Nitrogen adsorption–desorption measurements were conducted at 77 K with a Quantachrome (ASIQ MP) instrument. The powders were outgassed in vacuum at 250 °C for 4 h prior to the measurement. The surface area was obtained using Brunauer–Emmet–Teller (BET) method within the relative pressure ($P/P_0$) range of

0.05–0.20 and the pore size distributions (PSDs) were calculated by Barret–Joyner–Halenda (BJH) method. The nitrogen adsorption volume at the relative pressure ($P/P_0$) of 0.99 was used to determine the pore volume. The samples were imaged by a transmission electron microscopy, TEM using a Tecnai G2 30ST (FEI) instrument operating at 300 kV. For TEM analysis the powder samples were dispersed in ethanol by moderate sonication followed by dropping on the carbon-coated copper grid.

### 2.3. Congo red adsorption

For adsorption experiments with Congo red, in a typical experiment, 20 mg of the as-prepared M-$\gamma$A was mixed with 20 mL of aqueous solution of CR (100 mg L$^{-1}$) under vigorous stirring at room temperature. Analytical sample was taken from the suspension after different adsorption times and separated by centrifugation (5000 rpm). The supernatant solutions were analyzed with UV–vis spectroscopy (Varian, Cary 50) to obtain the concentration of CR in solution. The characteristic absorption of CR at around 500 nm was selected to monitor the adsorption process. The concentrations of CR were determined using a linear calibration curve over 6.25–100 mg L$^{-1}$ based on the absorbance value at 500 nm. The quantity ($q_t$) of CR adsorbed (mg CR/g adsorbent) by the sample (adsorbent) was determined as: $q_t = (C_0 - C_t)V/m$, where $C_0$ and $C_t$ are the initial and time ($t$) CR concentration (mg L$^{-1}$), respectively, $V$ is the volume of solution (mL), and $m$ is the sorbent weight (g) in dry form.

## 3. Results and discussion

### 3.1. Thermal analysis

Fig. 1 shows TG and DTA curves of the as-prepared powders obtained from (a) normal EISA and (b) solvothermal-assisted EISA (SA-EISA at 100 °C) processes. In the DTA curves, the endothermic peaks at 121 °C for EISA and at 115 °C for SA-EISA were attributed to the removal of adsorbed water. The sharp exothermic peaks at 239 °C for EISA and 258 °C for SA-EISA were due to the decomposition of organic surfactants [19]. Thermal decomposition temperature of the surfactant (Pluronic P123) was slightly more for SA-EISA compared to EISA; it was because of nonuniform distribution of the pores (sponge-like) generated by the surfactant (Pluronic P123) via the solvothermal reaction (discussed later). The thermal stability of the samples obtained by EISA and SA-EISA was confirmed by DTA analysis. The appearance of exothermic peak at around 885 °C for the sample obtained by conventional EISA could be ascribed to the transformation of $\gamma$-$Al_2O_3$ to $\theta/\alpha$-$Al_2O_3$. However, in XRD pattern (discussed shortly), the phase transformation was not clearly observed at 900 °C, but became evident at 1000 °C. Interestingly, it was noticed that for the sample obtained by SA-EISA, no such exothermic peak was observed at around 800–1000 °C. It confirmed that the SA-EISA sample was more thermally stable than that of EISA sample. The TG curves for the samples obtained by (a) EISA and (b) SA-EISA show a sharp decrease in weight loss of 69.5% and 60.3%, respectively up to 400 °C, which corroborated to the removal of water, hydroxides and organic surfactants (P123).

### 3.2. XRD characterization

Fig. 2 shows the XRD patterns of the calcined powders obtained from (a) EISA and (b) SA-EISA (100 °C) processes. It was observed that for EISA-based samples, $\gamma$-$Al_2O_3$ phase (JCPDS File No. 10-425) was observed up to 900 °C following a little transformation to $\theta$-$Al_2O_3$ (JCPDS File No. 35-121) and $\alpha$-$Al_2O_3$ (JCPDS File No. 48-366) at 1000 °C; the latter phase ($\alpha$-$Al_2O_3$) transformed fully
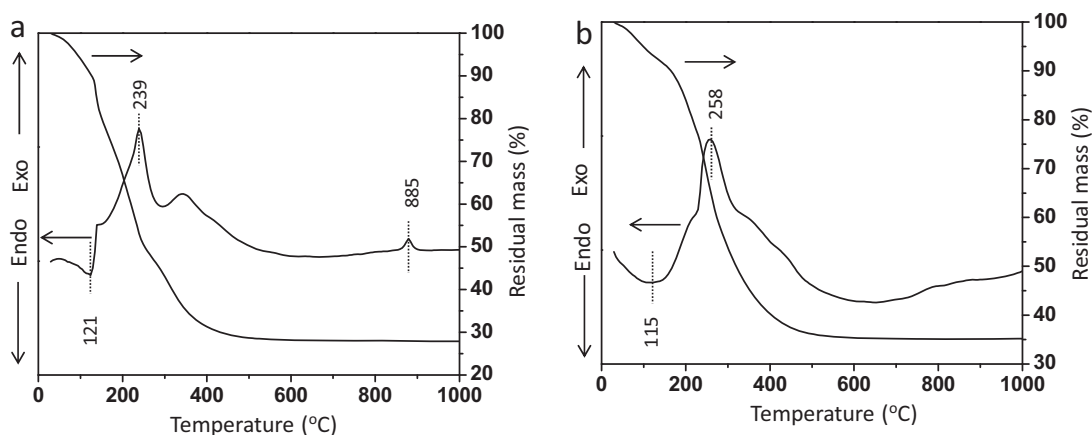
**Fig. 1.** TG and DTA curves of the gel powders obtained by (a) EISA and (b) SA-EISA (100 °C) processes.
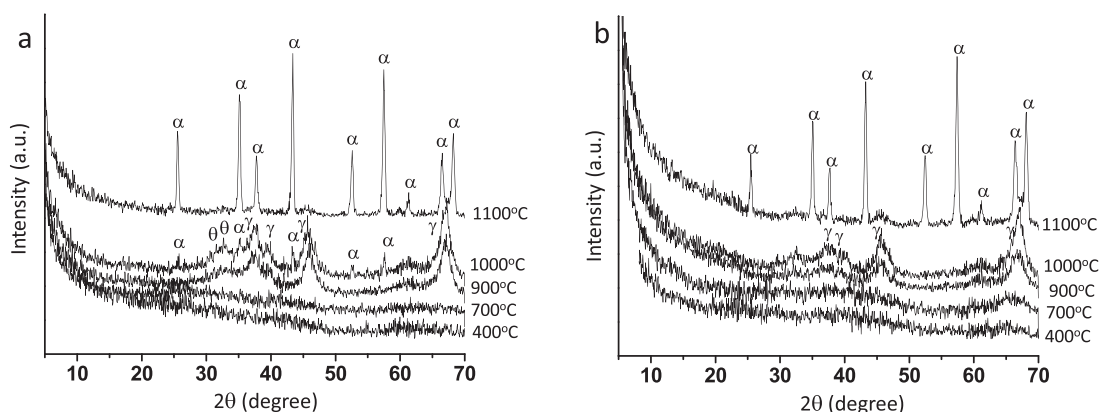


**Fig. 2.** XRD patterns of the powders obtained by (a) EISA and (b) SA-EISA (100 °C) processes. γ: γ-alumina; θ: θ-alumina; α: α-alumina
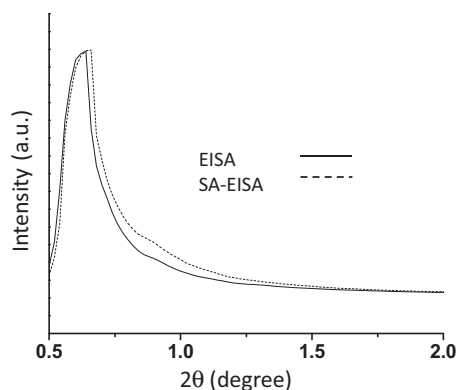


**Fig. 3.** Low-angle XRD patterns of the powders obtained by EISA and SA-EISA (100 °C) processes.

at 1100 °C. Interestingly, for the sample obtained by SA-EISA process, the $\gamma$-$Al_2O_3$ phase became stable up to 1000 °C followed by the transformation to $\alpha$-$Al_2O_3$ at 1100 °C. Therefore, $\gamma$-$Al_2O_3$ phase obtained by SA-EISA was more thermally stable than that prepared from EISA process. These results also corroborated with the DTA results. The low-angle XRD patterns (Fig. 3) of the 400 °C-treated powders obtained by EISA and SA-EISA (100 °C) processes exhibited $2\theta$ peaks at 0.62 ($d_{100}$ = 14.25 nm) and 0.64 ($d_{100}$ = 13.80 nm), respectively, which indicated the presence of mesopores in the samples. For the sample SA-EISA, a slight shifting of the low-angle peak to higher value accompanying with a lower $d$-spacing

reflected a lesser organization of pores [20] along with larger pore diameter [21] compared to those for the sample prepared by EISA process. It was supported by the textural and microstructural properties (discussed shortly).

### 3.3. $N_2$ adsorption–desorption studies

To investigate the effect of solvothermal reaction temperatures on the surface textural properties of the powders, the 400 °C-treated samples obtained at the synthesis temperature of 80 °C, 100 °C and 130 °C were analyzed with $N_2$ adsorption–desorption studies. Fig. 4 shows (a) $N_2$ adsorption–desorption isotherms and (b) PSDs of the samples prepared at different solvothermal reaction temperatures. It indicated that the powders prepared at 100 °C rendered higher BET surface area, pore volume and pore size compared to those obtained at 80 °C and 130 °C, which is clear from Table 1. Table 1 also exhibits that the samples prepared at 80 °C contained microporosity along with mesoporosity. It is worth mentioning that for dye adsorption efficiency with mesoporous alumina, the higher surface area, pore volume and porosity of the samples are the important parameters. In the present study, the solvothermal reaction temperature at 100 °C was found to be optimum in terms of higher textural properties (surface area, pore volume and pore size). Therefore, a comparative study was performed with the samples prepared by SA-EISA process at 100 °C and those obtained by conventional EISA process. Fig. 5 shows the $N_2$ adsorption–desorption isotherms of the powders obtained by (a) EISA and (b) SA-EISA (100 °C) processes followed by calcination at 400 °C, 700 °C, 900 °C,
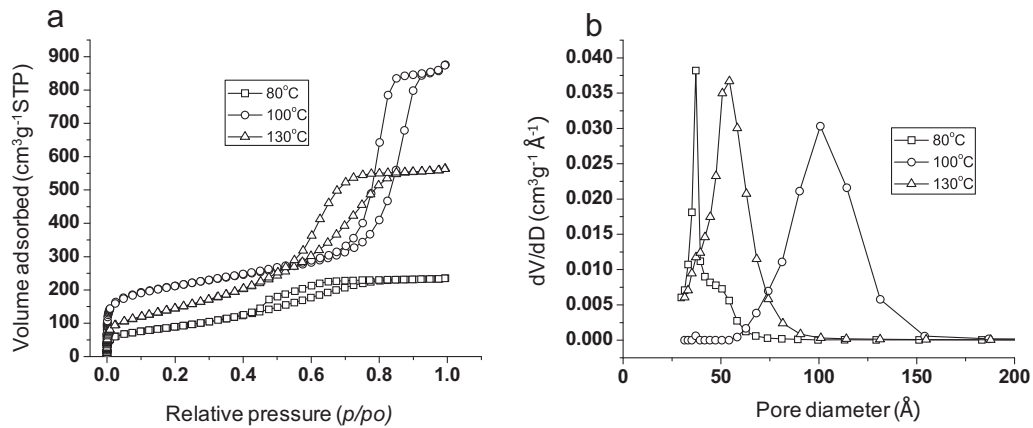
**Fig. 4.** (a) Nitrogen adsorption–desorption isotherms of mesoporous γ-alumina obtained by SA-EISA process at 80 °C, 100 °C and 130 °C, and (b) pore size distributions of the corresponding samples.

**Table 1**
Textural properties of the powders obtained by SA-EISA process at different solvothermal reaction temperatures.

| Reaction temperature (°C) | $S_{BET}$ (m² g⁻¹)[a] | $S_{External}$ (m² g⁻¹)[b] | $S_{Micropore}$ (m² g⁻¹)[c] | $V_{p\text{-Total}}$ (cm³ g⁻¹)[d] | $V_{p\text{-Micropore}}$ (cm³ g⁻¹)[e] | Pore diameter (nm)[f] |
|---|---|---|---|---|---|---|
| 80 | 322.5 | 253.7 | 68.8 | 0.365 | 0.037 | 3.72 |
| 100 | 742.9 | 742.9 | 0 | 1.355 | 0 | 10.08 |
| 130 | 524.0 | 524.0 | 0 | 0.875 | 0 | 5.45 |

[a] BET surface area.
[b] External surface area.
[c] Micropore surface area.
[d] Total pore volume.
[e] Micropore volume.
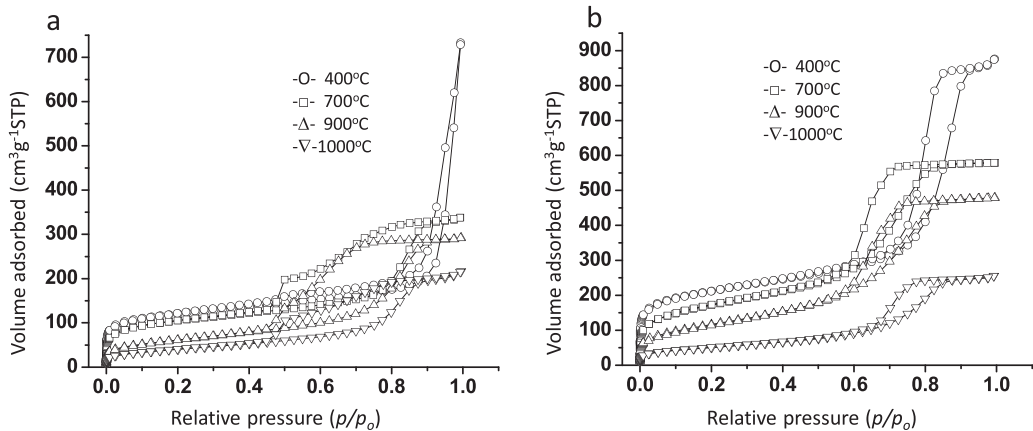[f] Pore diameter by BJH desorption.



**Fig. 5.** Nitrogen adsorption–desorption isotherms of mesoporous γ-alumina obtained by (a) EISA and (b) SA-EISA (100 °C) processes.
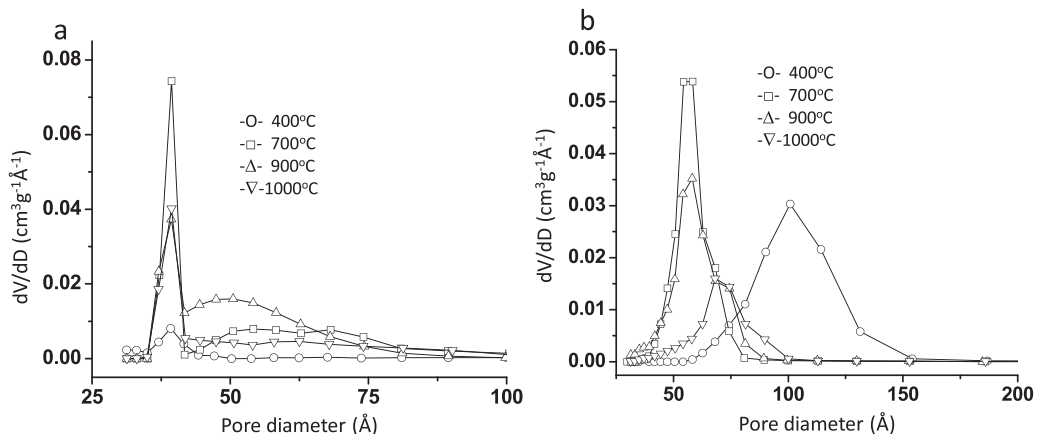


**Fig. 6.** Pore size distributions of mesoporous γ-alumina obtained by (a) EISA and (b) SA-EISA (100 °C) processes.

1000 °C and 1100 °C. It was noticed that all the curves displayed type IV isotherm according to IUPAC classification, which indicated mesoporous characteristic of the sample. For 400 °C-treated EISA sample, a steep increase in adsorption occurred from a $P/P_0$ of about 0.9. The $N_2$ adsorption–desorption isotherms of SA-EISA process (Fig. 5b) also shows type IV isotherms with a distinct condensation step at a $P/P_0$ range of 0.6–0.9. With increase in calcination temperatures, the decrease sizes of the hysteresis loops indicated lesser amount of capillary condensation in the mesopores. Fig. 6 shows the BJH pore size distributions (PSD) of the powders obtained by (a) EISA and (b) SA-EISA (100 °C) processes. It was noticed that for the samples prepared by EISA process, the pore size centered at around 4 nm, while the samples prepared by SA-EISA rendered the pore size at around 6–7 nm. However, 400 °C-treated samples prepared by SA-EISA exhibited a significant increase in pore size of about 10 nm. The textural properties (BET surface area, total pore volume and pore diameter) of the powders obtained by the EISA and SA-EISA (100 °C) processes after calcination at different temperatures are shown in Table 2. With increase in calcination temperatures, the BET surface area and pore volume decreased for both the samples EISA and SA-EISA. It was due to the collapse of the pores at higher temperatures. It is interesting to notice that a significant increase in BET surface area and total pore volume were obtained from SA-EISA samples for all the calcinations temperatures. For SA-EISA at 400 °C, the BET surface area was 742.9 m$^2$ g$^{-1}$, and that for the sample EISA at 400 °C, it was 419.6 m$^2$ g$^{-1}$. Therefore, the significant increase in BET surface area for SA-EISA samples was attributed to

**Table 2**
Textural properties of the powders obtained by (a) EISA and (b) SA-EISA (100 °C) processes.

| Sample (calcination temperature (°C)) | $S_{BET}$ (m$^2$ g$^{-1}$)[a] | $V_{p\text{-Total}}$ (cm$^3$ g$^{-1}$)[b] | $D_p$ (nm)[c] |
|---|---|---|---|
| EISA (400) | 419.6 | 1.134 | 3.92 |
| EISA (700) | 371.4 | 0.5227 | 3.93 |
| EISA (900) | 220.9 | 0.4520 | 3.93 |
| EISA (1000) | 146.6 | 0.3353 | 3.94 |
| SA-EISA (400) | 742.9 | 1.355 | 10.08 |
| SA-EISA (700) | 616.5 | 0.8959 | 5.83 |
| SA-EISA (900) | 422.8 | 0.7408 | 5.81 |
| SA-EISA (1000) | 182.6 | 0.3949 | 6.82 |

[a] BET surface area.
[b] Total pore volume.
[c] Pore diameter by BJH desorption.

the more abundance of mesopores generated under solvothermal reaction (SA-EISA process). Table 2 also shows that pore sizes of the samples prepared by SA-EISA were more than those obtained by EISA method. Under solvothermal reaction at 100 °C, pore enlargement occurred with the surfactant, Pluronic P123 in the presence of the solvent (ethanol), which became restricted in the conventional EISA process. More solvent molecules entrapped into the gel network under solvothermal process enhancing the pore properties of the samples.
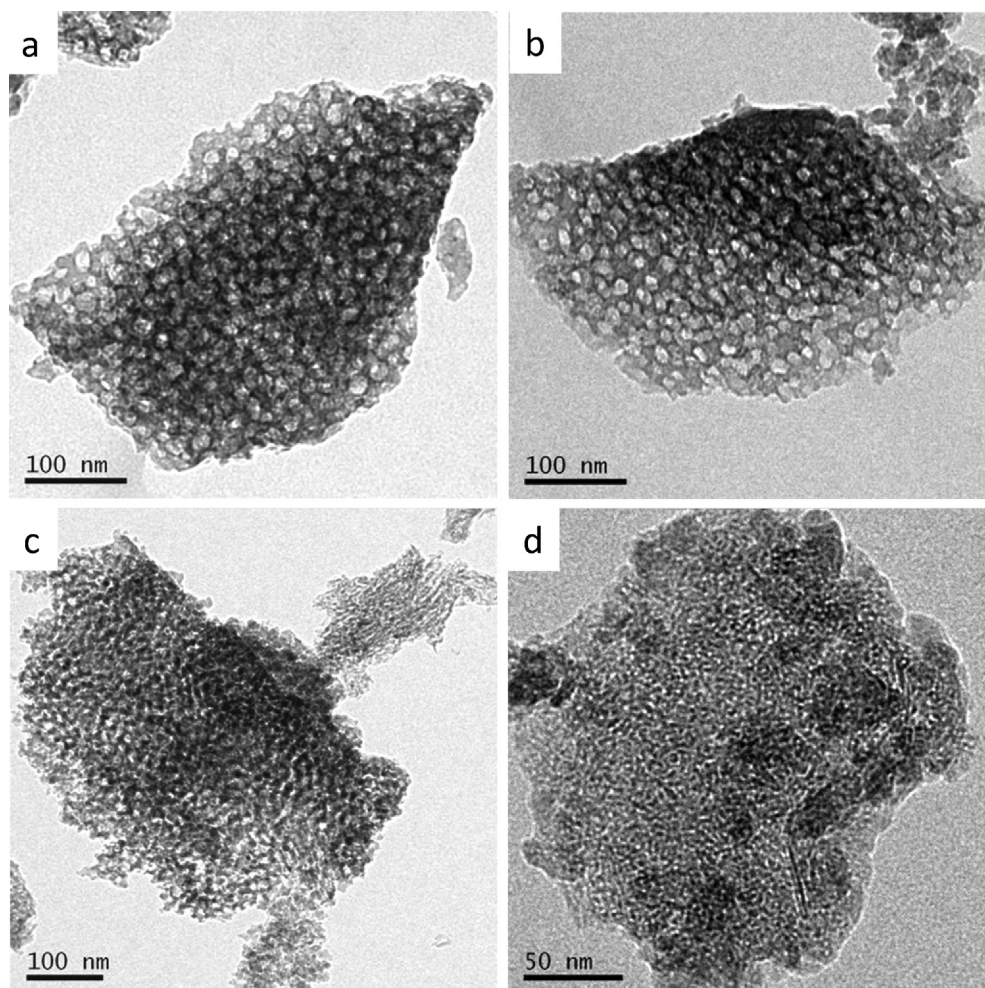


**Fig. 7.** TEM images of mesoporous γ-alumina obtained by EISA process followed by calcination at (a) 400 °C, (b) 700 °C, (c) 900 °C, and (d) 1000 °C.
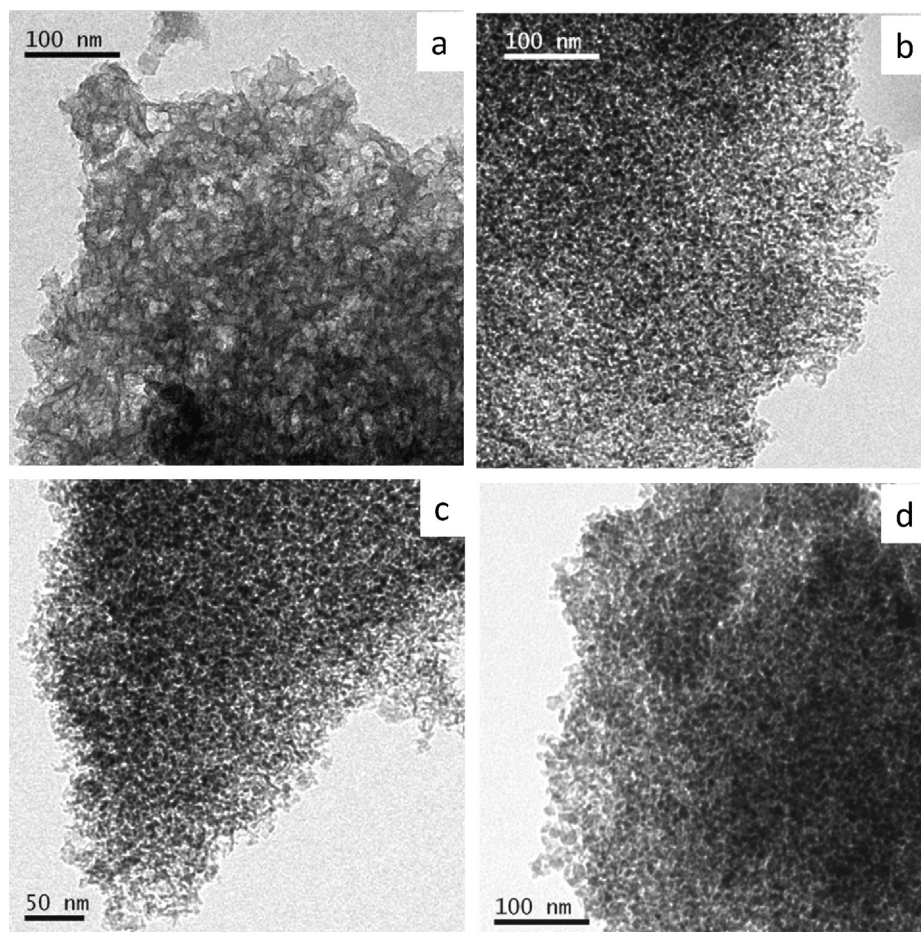
**Fig. 8.** TEM images of mesoporous γ-alumina obtained by SA-EISA (100 °C) process followed by calcination at (a) 400 °C, (b) 700 °C, (c) 900 °C, and (d) 1000 °C.

### 3.4. Microstructural studies

Fig. 7 shows the TEM images of the samples obtained from EISA process followed by calcination at (a) 400 °C, (b) 700 °C, (c) 900 °C and (d) 1000 °C. The worm-like mesostructures of the samples were found for 400 °C and 700 °C-treated samples. With increase in calcination temperatures at 900–1000 °C, sponge-like mesoporous structure was noticed. However, under solvothermal reaction (SA-EISA) at 100 °C, sponge-like microstructure was obtained for all the temperatures (Fig. 8). It is believed that under autogenic pressure at 100 °C of solvothermal reaction, the entropy of the system was high having random movement of the colloidal particles in the system. It hindered for the generation of uniform pore structures. Under solvothermal reaction, the randomness of particle movement enhanced the abundance of pores with larger pore sizes resulting in higher BET surface area, pore volume and pore size compared to those obtained from conventional EISA method.

### 3.5. Adsorption property for Congo red

Fig. 9 shows UV–vis absorption spectroscopy measurements of the 400 °C-treated samples prepared by (a) EISA and (b) SA-EISA (100 °C) processes for the determination of CR concentration before and after adsorption. It demonstrates that for both the samples with increasing time, the absorbance values decreased indicating decreased concentration of CR, which signified adsorptivity of the samples. This effect became more pronounced for the sample prepared by SA-EISA process. Fig. 9c shows the change of adsorption capacity with time. The adsorption capacity for both the samples

(EISA and SA-EISA) increased sharply up to 90 min. However, the adsorption capacities of about 70 mg/g and 100 mg/g were obtained after 120 min for the samples prepared by EISA and SA-EISA, respectively. It is clear that the sample prepared by SA-EISA process exhibited higher adsorption capacity for Congo red as compared to that prepared by EISA process. The higher BET surface area and pore volume as well as larger pores for the sample obtained from SA-EISA process caused for higher adsorption capacity for Congo red [22].

### 3.6. Formation mechanism

Fig. 10 depicts a tentative mechanism for the formation of worm-like mesostructures for the sample prepared by EISA, and sponge-like mesostructures for the sample prepared by SA-EISA. In EISA process, surfactant (P123) concentration increases with evaporation of solvent (ethanol), which drives self-assembly of alumina-surfactant micelles. In alumina-surfactant micelle, hydrophobic polypropylene oxide (PPO) moieties of the surfactant remain in the core surrounded by hydrophilic polyethylene oxide (PEO) moieties in the corona. The hydroxyl (–OH) groups in the alumina sol particles obtained by the hydrolysis of aluminum isopropoxide in acidic medium interact with the hydrophilic polyethylene oxide (PEO) of the surfactant molecules through hydrogen bonding. It was reported that alkylene oxide segments can form crown-ether-type complexes with inorganic metal ions through weak coordination bonding [6]. Therefore, in the present case both the hydrogen bonding and coordination interactions could exist between the surfactant and alumina particles. With
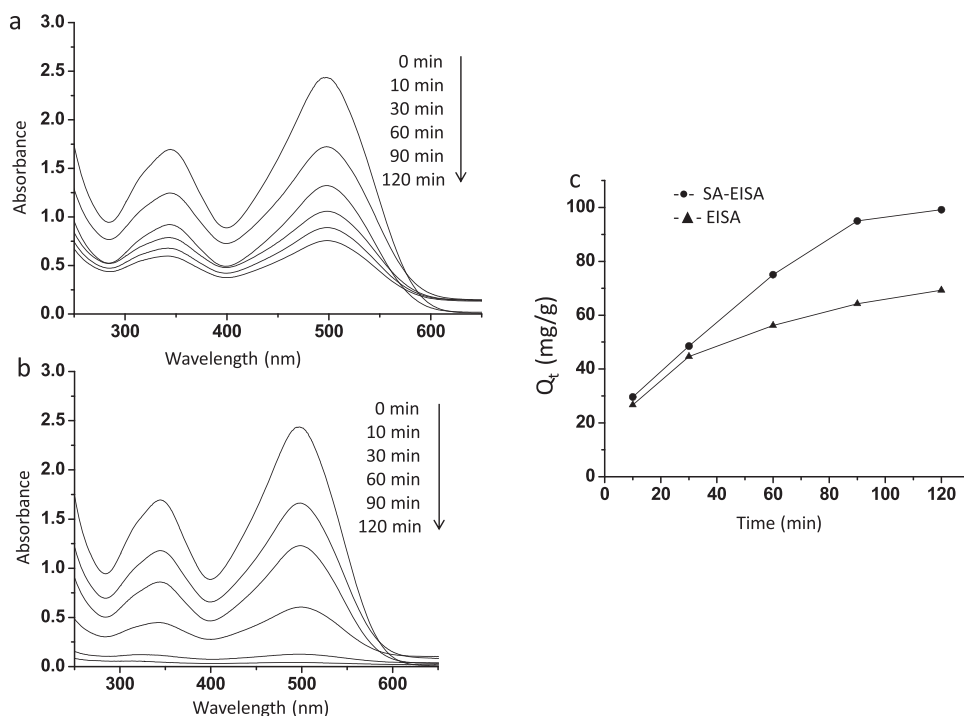
**Fig. 9.** Absorption spectra of CR after different time intervals using mesoporous γ-alumina obtained by (a) EISA and (b) SA-EISA (100 °C) processes, and (c) their adsorption capacities for Congo red, after calcination at 400 °C/4 h each.
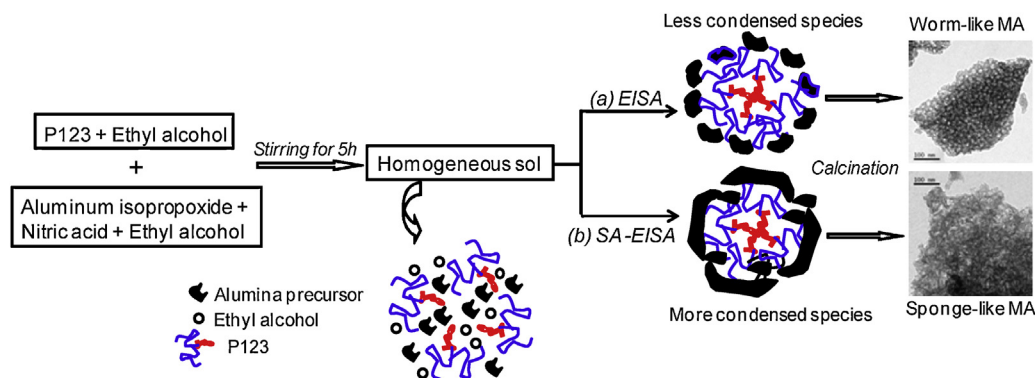


**Fig. 10.** Schematic representation for the formation of mesoporous γ-alumina (MA) obtained by (a) EISA and (b) SA-EISA processes.

slow evaporation of the solvent (by EISA process), self-organization of micelles results in the formation of final mesostructure. It has been reported [23] that EISA process is governed by both the kinetic processes of (a) condensation of inorganic species (alumina) and (b) alumina-surfactant micelle organization, which are influenced by the removal of volatile species (solvent). However, it is difficult to predict whether the above processes occur successively or simultaneously during drying. Under solvothermal condition, a jelly-like mass composed of alumina precursor, surfactant and solvent was obtained. It demonstrates that under solvothermal condition, higher degree of condensation of alumina species takes place before solvent evaporation via EISA. With more condensed species of alumina, the micelles are randomly arranged yielding disordered structure (spongy) under solvothermal-assisted EISA process. After thermal decomposition, elimination of template molecules renders worm-like mesopores for conventional EISA-treated samples, and disordered (spongy) mesopores for SA-EISA-treated samples. It is to be noted that under autogenic pressure at 100 °C, the weakening of noncovalent interaction (e.g. hydrogen bonding) causes the expansion of inorganic framework resulting in larger pore size.

## 4. Conclusions

The effect of solvothermal reaction on the physico-chemical properties of solvothermal-assisted EISA-based mesoporous γ-$Al_2O_3$ was investigated. The γ-$Al_2O_3$ prepared by solvothermal-assisted EISA process was thermally more stable up to 1000 °C, while the same prepared by conventional EISA process is stable up to 900 °C. A significant increase in textural properties (BET surface area, pore volume and pore size) was noticed under solvothermal reaction condition. The more abundance of pores accompanying with higher BET surface area and pore volumes for solvothermal-assisted sample rendered higher adsorption capacity for Congo red compared to that for the sample prepared in the absence of solvothermal reaction.

## References

[1] C.T. Kresge, M.E. Leonowicz, W.J. Roth, J.C. Vartuli and J.S. Beck, Nature, 359, 710–712 (1992).

[2] F. Vaudry, S. Khodabandeh and M.E. Davis, Chem. Mater., 8, 1451–1464 (1996).

[3] V.V. Vinogradov, A.V. Agafonov, A.V. Vinogradov, T.I. Gulyaeva, V.A. Drozdov and V.A. Likholobov, J. Sol-Gel Sci. Technol., 56, 333–339 (2010).

[4] C. Boissiere, L. Nicole, C. Gervais, F. Babonneau, M. Antonietti, H. Amenitsch, C. Sanchez and D. Grosso, Chem. Mater., 18, 5238–5243 (2006).

[5] M. Trueba and S.P. Trasatti, Eur. J. Inorg. Chem., 17, 3393–3403 (2005).

[6] P. Yang, D. Zhao, D.I. Margolese, B.F. Chmelka and G.D. Stucky, Nature, 396, 152–155 (1998).

[7] K. Niesz, P. Yang and G.A. Somorjai, Chem. Commun., 15, 1986–1987 (2005).

[8] Q. Liu, A. Wang, X. Wang and T. Zhang, Chem. Mater., 18, 5153–5156 (2006).

[9] Z. Zhang and T.J. Pinnavaia, Angew. Chem. Int., 47, 7501–7504 (2008).

[10] M. Rodriguez, A.B. Sifontes, F.J. Mendez, Y. Diaz, E. Canizales and J.L. Brito, Ceram. Int., 39, 4499–4506 (2014).

[11] C. Liu, Y. Liu, Q. Ma and H. He, Chem. Eng. J., 163, 133–142 (2010).

[12] Z. Obrenovic, M. Milanovic, R.R. Djenadic, I. Stijepovic, K.P. Giannakopoulos, M. Perusic and L.M. Nikolic, Ceram. Int., 37, 3253–3263 (2011).

[13] S. Ghosh, R. Dalapati and M.K. Naskar, J. Asian Ceram. Soc., 2, 380–386 (2014).

[14] Q. Yuan, A.X. Yin, C. Luo, L.D. Sun, Y.-W. Zhang, W.-T. Duan, H.-C. Liu and C.-H. Yan, J. Am. Chem. Soc., 130, 3465–3472 (2008).

[15] G.J.A.A. Soler-Illia, C. Sanchez, B. Lebeau and J. Patarin, Chem. Rev., 102, 4093–4138 (2002).

[16] M.K. Naskar and M. Eswaramoorthy, J. Chem. Sci., 120, 181–186 (2008).

[17] S. Ghosh, K.P. Dey and M.K. Naskar, J. Am. Ceram. Soc., 96, 28–31 (2013).

[18] S. Ghosh and M.K. Naskar, J. Am. Ceram. Soc., 96, 1698–1701 (2013).

[19] M. Kurahashi, K. Kanamori, K. Takeda, H. Kaji and K. Nakanishi, RSC Adv., 2, 7166–7173 (2012).

[20] J.C. Ray, K.-S. You, J.-W. Ahn and W.-S. Ahn, Microporous Mesoporous Mater., 100, 183–190 (2007).

[21] X. Liu, Y. Wei, D. Jin and W.-H. Shih, Mater. Lett., 42, 143–149 (2000).

[22] C. Yu, X. Dong, L. Guo, J. Li, F. Qin, L. Zhang, J. Shi and D. Yan, J. Phys. Chem. C, 112, 13378–13382 (2008).

[23] D. Grosso, F. Cagnol, G.J.deA.A. Soler-Illia, E.L. Crepaldi, H. Amenitsch, A. Brunet-Bruneau, A. Bourgeous and C. Sanchez, Adv. Funct. Mater., 14, 309–322 (2004).